Journal of Colloid and Interface Science 364 (2011) 505–511

Contents lists available at SciVerse ScienceDirect

Journal of Colloid and Interface Science

www.elsevier.com/locate/jcis

Effect of disjoining pressure on terminal velocity of a bubble sliding along an inclined wall

Lorena A. Del Castillo [a], Satomi Ohnishi [a,*], Lee R. White [b], Steven L. Carnie [c], Roger G. Horn [d]

[a] Ian Wark Research Institute, University of South Australia, Mawson Lakes, SA 5095, Australia
[b] School of Mathematics and Statistics, University of South Australia, Mawson Lakes, SA 5095, Australia
[c] Department of Mathematics and Statistics, The University of Melbourne, Victoria 3010, Australia
[d] Institute of Technology Research and Innovation, Deakin University, 221 Burwood Highway, Victoria 3125, Australia

ARTICLE INFO

Article history:
Received 14 January 2011
Accepted 19 August 2011
Available online 26 August 2011

Keywords:
Sliding bubble
Terminal velocities
Disjoining pressure
Hydrodynamic forces
Double-layer forces
Electrolyte concentration

ABSTRACT

The influence of salt concentration on the terminal velocities of gravity-driven single bubbles sliding along an inclined glass wall has been investigated, in an effort to establish whether surface forces acting between the wall and the bubble influence the latter's mobility. A simple sliding bubble apparatus was employed to measure the terminal velocities of air bubbles with radii ranging from 0.3 to 1.5 mm sliding along the interior wall of an inclined Pyrex glass cylinder with inclination angles between 0.6 and 40.1°. Experiments were performed in pure water, 10 mM and 100 mM KCl solutions. We compared our experimental results with a theory by Hodges et al. [1] which considers hydrodynamic forces only, and with a theory developed by two of us [2] which considers surface forces to play a significant role. Our experimental results demonstrate that the terminal velocity of the bubble not only varies with the angle of inclination and the bubble size but also with the salt concentration, particularly at low inclination angles of ~1–5°, indicating that double-layer forces between the bubble and the wall influence the sliding behavior. This is the first demonstration that terminal velocities of sliding bubbles are affected by disjoining pressure.

1. Introduction

Many industrial processes such as mineral flotation, water treatment, and emulsification, are carried out under conditions of multiphase flow, in which bubbles play a key role in determining the process efficiency. Hence, the motion of bubbles in different configurations has been studied extensively in order to understand the kinetics of bubbles interacting with solid surfaces. A large number of studies has been conducted on vertically rising bubbles in unbounded or confined geometries [3–22] which have provided insights on air–liquid interfaces of free rising bubbles and bubbles influenced by solid surfaces. Since a lot of processes in reality involve not only vertical movement of bubbles but also bubble motion along angled surfaces in liquid media, studies of bubbles moving parallel to inclined surfaces [23–41] are also of significant interest in different fields such as engineering, medicine and various industries including petroleum and food.

To understand the kinetics of bubbles sliding along solid surfaces, it is essential to identify the relevant forces acting on the bubble. The only pertinent theory we found in the literature is that of Hodges et al. [1] which considers gravitational and hydrodynamic forces in predicting the behavior of drops sedimenting down a gently inclined plane. The theory determines the thickness h_o, of the thin liquid film separating the drop (or bubble) and the solid wall, from a normal force balance of buoyancy against hydrodynamic pressure forces. Hodges et al. compared the velocities predicted by their theory with an experimental study on air bubbles sliding along inclined planes in viscous liquid (silicone oil) performed by Aussillous and Quéré [31]. The velocities predicted by the theory of Hodges et al. were greater than the experimental measurements of Aussillous and Quéré, indicating that the theory has not captured all of the physics in this system.

Another type of force that could be affecting the sliding velocity, albeit indirectly, is a surface force acting between the bubble and the wall, such as a van der Waals force or an electrical double-layer repulsion. The effect of such forces, expressed as an additional "disjoining" pressure in the thin layer of liquid between the bubble and wall, would be to deform the bubble, thereby changing the hydrodynamic forces acting on it. Of course hydrodynamic forces can also deform the bubble, as discussed by Hodges et al., making a theory that incorporates both disjoining and hydrodynamic pressures quite complex.

A bare glass surface (without modification/capping by chemical reagents) in water (pH 5–7) is negatively charged, since the isoelectric point of glass is observed to be around pH 2 [42,43]. The surface potential of an air–water interface is generally negative [44–51]. Since glass surfaces and air–water interfaces are both

* Corresponding author. Fax: +61 8302 3755.
E-mail address: satomi.onishi@unisa.edu.au (S. Ohnishi).

0021-9797/$ - see front matter © 2011 Elsevier Inc. All rights reserved.
doi:10.1016/j.jcis.2011.08.046

negatively charged in water, one could expect some influence from electrical double layer interaction between them. Thus we think that disjoining pressure could play a role in the dynamics of a bubble sliding along inclined glass surfaces in aqueous liquid. To investigate this, we initiated a two-pronged attack based on experiments and theoretical development.

The theory assumes, as its starting point, that the bubble is effectively flattened by its DLVO interaction with the wall, so that the thickness h_o of a uniform thin film separating the bubble (approximated by a truncated sphere) is determined by the surface charges on the wall and the bubble, and the electrolyte concentration in the aqueous phase. The terminal velocity U_T of a bubble sliding along an inclined surface is found to depend on the radius A of the bubble, the angle of inclination ϕ of the surface, and h_o [2].

In parallel with the theoretical development, we also explored experimentally whether disjoining pressure has an effect on the terminal velocity of the sliding bubble in aqueous solutions. To achieve this we employed a simple sliding bubble apparatus to measure the terminal velocity of a bubble sliding under the force of gravity along an inclined surface in an aqueous medium, with various concentrations of electrolyte because this is well known to influence double-layer forces.

The body of literature on bubbles sliding along inclined surfaces in liquid mostly reports on effects of bubble size [27,31,33,37,40], bubble shape [25], size of liquid channel [24–26,30], angle of inclination [23–28,30,31,33,36–38,41], surfactants [33,34,40], gas type [40], liquid temperature [26,40,52], and other liquid properties [23,24,26,28,30,31,52] such as viscosity, density, and surface tension on the dynamics of the sliding bubble. However, salt concentrations of liquid media, to our knowledge, have not yet been a parameter of any study in bubbles sliding along inclined surfaces.

In this article we present our experimental observations on the effects of salt concentration together with that of the bubble size and angle of inclination on the terminal velocity of the sliding bubble. We also present a comparison between our experimental results and the two theories discussed above, those due to Hodges et al. [1] and White and Carnie [2].

2. Materials and methods

2.1. Sliding bubble apparatus

The sliding bubble apparatus employed in this study (Fig. 1) was the same device used in bubble coalescence experiments reported previously [53] to investigate the effects of salt concentration and speed of approach on the coalescence time of a bubble rising to meet the surface of the liquid. The experimental set-up consisted of a sealed graduated glass cylinder (100 ml, Pyrex, England), containing the liquid medium, attached parallel to a tilting platform. The cylindrical geometry ensures that the sliding bubble follows a straight path, while the internal diameter of the cylinder (37 mm) is large enough that curvature of the solid surface is negligible on the mm scale of the bubble. A Teflon cap sealing the cylinder had two holes: one where a long stainless steel needle (Hamilton, 26 s gauge, 38 mm long) is fitted and the other one (0.47 mm) acting as a very small air vent. A bubble, formed by turning the screw-threaded plunger of an airtight glass syringe (1 ml, Gastight #1001, Hamilton, USA), was released at the lower end of the cylinder via the needle and rose until it reached the cylinder wall. As the bubble slid up along the top wall of the cylinder, its size and terminal velocity were measured with the aid of a high speed camera (CMOS Ultra II, 1.3 megapixel with NMV-6 Navitar 6 mm f1.4 lens) attached to the platform. Images of bubbles sliding at the middle part of the cylinder where the bubble has already attained terminal velocity were captured with frame rates and spatial resolutions depending on the angle of inclination: 91 frames per second at a spatial resolution of 768 × 568 pixels for low angles of inclination (ϕ = 0.6–4.2°); and 147 frames per second at 500 × 550 pixels for higher angles (ϕ = 10–40°). Graduations on the outside of the cylinder were used to calibrate the camera magnification and to identify the position of the bubble as a function of time. The angle of inclination was varied by a screw mechanism, and determined by measuring the height of a laser spot, projected by a laser pointer attached parallel to the platform, at a known distance 1–2 m away from the pivot point. A backlight (white LED backlight NT57-820, Edmund Optics) and two soft fiber optic lights (Fibreoptic Illuminator Model 15001, Fibreoptic Lightguides, Australia) were positioned as shown in the figure to obtain sharp and shadowless bubble images.

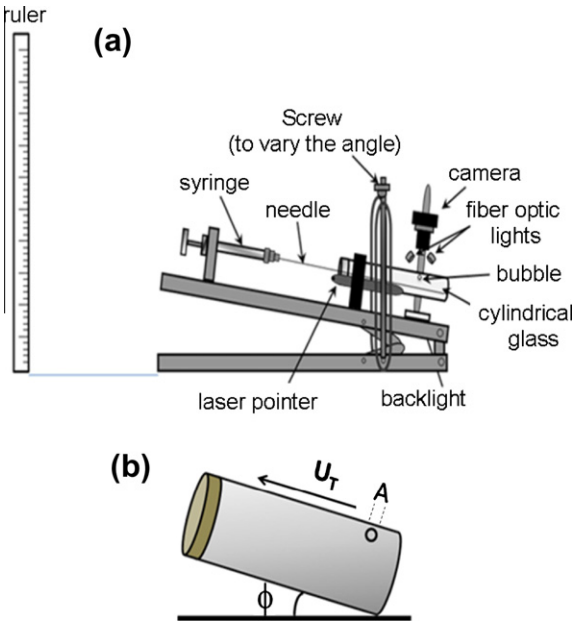

Fig. 1. Sliding bubble apparatus employed to generate bubbles sliding at different speeds and to measure their sizes and terminal velocities: (a) schematic illustration of the experiment; (b) an illustration showing the measurable parameters: angle of inclination, ϕ, bubble terminal velocity U_T, and bubble radius, A.

ImageJ freeware (Ver. 1.38x, downloaded from http://rsweb.nih.gov/download.html) was used to measure the size and speed of the bubbles. Estimated errors were ±0.02 mm in diameter; a maximum of ±0.1° in inclination angle for ϕ < 10° and a maximum of ±0.2° for ϕ > 10°. For the speed, estimated errors depend on the speed range: ±0.01 mm/s at very low speeds ($U_T \sim$ 1–3 mm/s); ±0.33 mm/s for $U_T \sim$ 10 mm/s; 7.1 mm/s for $U_T \sim$ 100 mm/s.

We determined U_T by monitoring the velocity of a bubble after it was released from the end of the needle. It was observed that the released bubble initially bounced several times or moved in a nonlinear (zigzag) path for a distance of ~10 mm before sliding parallel to the wall. When the bubble started sliding parallel to the wall the sliding velocity was unstable during the first ~40 mm of travel. For example, for a bubble with radius of 1.2 mm sliding along a wall inclined at ϕ = 5°, the speed varied from ~43 mm/s to 77 mm/s over a distance of ~40 mm. The sliding velocity was stabilised (~64 mm/s) after the bubble has travelled ~50 mm. Since all sliding velocities were stabilised at a distance of ~50 mm from the point the bubbles first touched the wall, we took the velocity at a distance of ~55 mm from that point as U_T.

2.2. Water, salt and cleaning procedures

Water was taken from a high-purity water system (MilliQ, Element) with a resistivity reading (while the water was still in the

MilliQ chamber) of 18.2 MΩ cm. Surface tension of the resultant water was 72.7 mN/m at 22.1 °C. "Fresh" water refers to freshly collected high purity (MilliQ) water. "Aged" water refers to MilliQ water that has been stored in the sealed glass cylinder for 5 days. The potassium chloride (Sigma–Aldrich, Analytical Reagent) used to make up electrolyte solutions was calcined for 9 h at 550 °C to remove possible organic trace contaminants followed by recrystallization and re-calcination for 14 h at 550 °C. All glassware and the Teflon cap, pre-cleaned with high purity water, were immersed in a 1 M KOH solution for 1.5 h and thoroughly rinsed with copious amounts of high purity water. The stainless steel needle, pre-cleaned with high purity water, was immersed in 10% HNO_3 for at least 30 min. After the process, the needle was rinsed thoroughly with high purity water and kept in ethanol (100% undenatured, Analytical Reagent) before use.

3. Results and discussion

3.1. Effects of inclination angle and bubble size on terminal velocity of the bubble

The speed of single bubbles sliding along the underside of an inclined surface has been measured for inclination angles from 0.6° to 40.1° in different salt concentrations. Fig. 2 shows all experimental data measured for inclination angles less than 5°. The data for higher angles (10–40°) are plotted in Fig. 3. These figures illustrate two predictable features.

The first feature is that, in the range of bubble size and inclination angle studied, the terminal velocity U_T increases as inclination angle is increased. This is because the buoyancy force acting parallel to the motion of the bubble sliding under an inclined surface is dependent on the sine of the angle. This trend has been observed by several researchers [23,25–28,31,37,52,54,55] from their experiments using a wide range of bubble radius from the smallest of ~0.85 mm by Masliyah and his co-workers [28] to elongated bubbles with equivalent radius of ~2.4 cm by Zukoski [23] and by Maxworthy [27]. In their independent studies, both Zukoski [23] and Maxworthy [27] observed a maximum velocity at an inclination angle of 45°. We note in Fig. 2a and b that for small bubbles ($A \sim 0.3$–0.7 mm) the increase in U_T with ϕ is minimal (~1–4 mm/s/°) whereas for the bigger bubbles ($A \sim 0.8$–1.5 mm) the increase in U_T is more significant (~6–36 mm/s/°). Perron et al. [37] studied the influence of ϕ on U_T for larger bubbles with radii of ~4–12.5 mm at inclination angles of 2–10°, and reported more complex behavior for these more deformable bubbles.

The second feature is the increase in bubble terminal velocity U_T as the size of the bubble is increased. Although not simple to calculate for a sliding bubble, the terminal velocity for a bubble far from the wall is proportional to the square of its radius, as explained by a simple force balance between the Stokes drag force $F_d = -3\pi\eta A U_T$ (η is the dynamic viscosity) being proportional to A, and the buoyancy force F_b being proportional to A^3: $F_b = (\pi g \Delta\rho A^3)/6$ ($\Delta\rho$ is the density difference between medium and particle, g is the gravitational constant). The values of U_T thus estimated from Stokes' law (assuming low Reynolds numbers: $U_T = A^2\Delta\rho g/18\eta$ for ϕ = 3.6°, 4.2°, and 40.1° are shown in Figs. 2 and 3. This calculation assumes immobile boundary conditions at the air–water interface (see next section). Assuming mobile boundary conditions would result in calculated terminal velocities being 50% higher.

3.2. The terminal velocity of the bubble in fresh and aged water

An interesting feature observed at the angles between 2.1° and 4.2° (Fig. 2) is that freshly collected Milli-Q water exhibited a slightly higher U_T compared to the Milli-Q water which has been stored for 5 days in the closed glass chamber. Note that correlation coefficients (R^2) of the trend lines for water at 3.6° and 4.2° are 0.998 and 0.999. A possible explanation is that over time, trace amount of impurities could have entered the water through the small air vent or by leaching out of the glass. The introduction of even a very small amount of impurity (surfactant/ion) into the clean water could alter the boundary condition at the air–water interface, from fully mobile which is expected for ultra-clean water, particularly at this speed range ($U_T \sim$ 10–50 mm/s) as we have shown in a separate study on bubble coalescence [53], to partially or fully-immobile. The presence of trace amounts of surface-active contaminants/ions could cause surface tension gradients to develop along the surface of the bubble or on the thin liquid film between the bubble and the glass wall as a result of the coupling between flow and surface concentration distribution of the ions/contaminants. This could cause partial immobilization of the bubble's surface and eliminate internal circulation, thereby significantly increasing the drag, as discussed by Clift et al. [56], leading to a decrease in the bubble's speed. This phenomenon

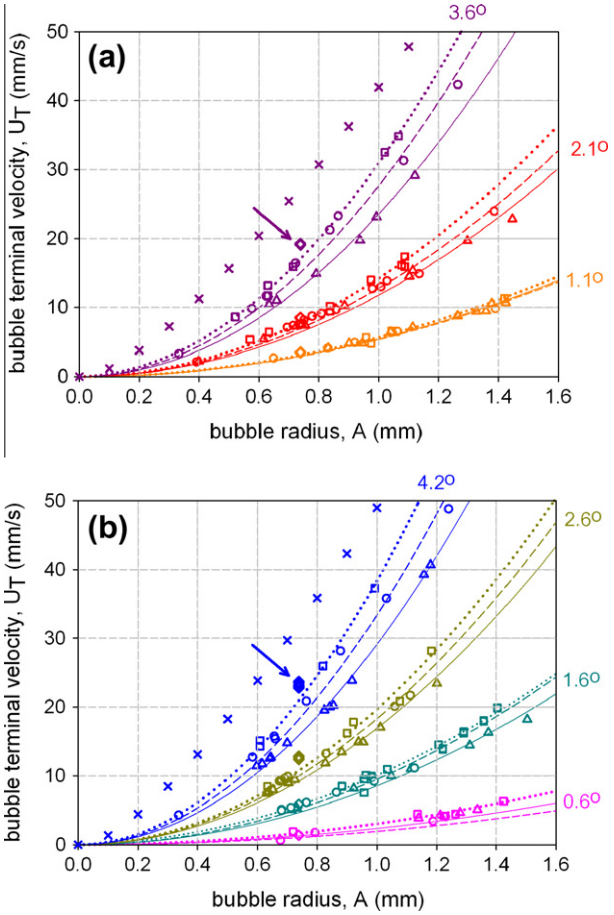

Fig. 2. Bubble terminal velocity versus bubble size in different salt concentrations: fresh Milli-Q water (diamonds: with arrows for 3.6° and 4.2°), 5 day-old Milli-Q water (squares), 10 mM KCl (circles), 100 mM KCl (triangles) and estimated values from Stoke's law at low Reynolds numbers for 3.6° and 4.2° (crosses). For better visual clarity, the data has been divided into two groups by angle of inclination: (a) 1.1°, 2.1°, 3.6°; and (b) 0.6°, 1.6°, 2.6 °, 4.2°. Trend lines are least squares second-order polynomial fits to sets of data points: dotted lines for 5 day-old Milli-Q water: dashed lines for 10 mM KCl: and solid lines for 100 mM KCl. The correlation coefficient (R^2) for each line is: (a) 0.974 (1.1°), 0.988 (2.1°), 0.998 (3.6°) for water; 0.958 (1.1°), 0.991 (2.1°), 0.993 (3.6°) for 10 mM KCl; 0.988 (1.1°), 0.997 (2.1°), 0.996 (3.6°) for 100 mM KCl: (b) 0.946 (0.6°), 0.983 (1.6°), 0.998 (2.6°), 0.999 (4.2°) for water; 0.990 (0.6°), 0.997 (1.6°), 1.000 (2.6°), 0.997 (4.2°) for 10 mM KCl; 0.999 (0.6°), 0.997 (1.6°), 0.999 (2.6°), 0.996 (4.2°) for 100 mM KCl. Note that there is a limited range of bubble size using the freshly-prepared Milli-Q water thus fitting a line to each set was not possible.

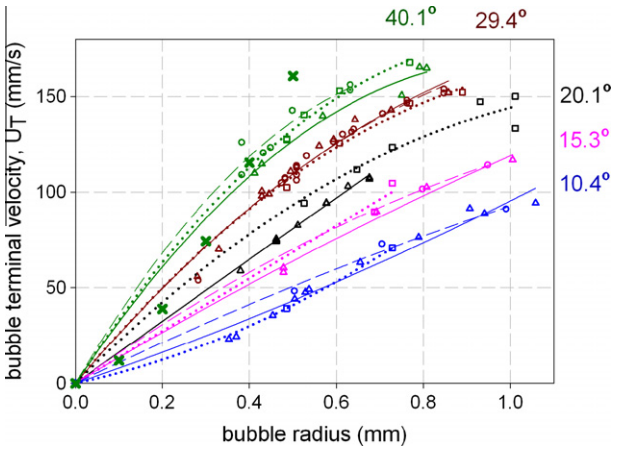

Fig. 3. Bubble terminal velocity versus bubble size for higher angles of inclination (ϕ between 10.4° and 40.1°) for different salt concentrations: water (squares), 10 mM KCl (circles), 100 mM KCl (triangles), and estimated values from Stoke's law at low Reynolds numbers for 40.1° (crosses). Trend lines are least squares second-order polynomial fits to sets of data points: dotted lines for water: dashed lines for 10 mM KCl: and solid lines for 100 mM KCl. The correlation coefficient (R^2) for each line is: 0.912 (10.4°), 0.607 (15.3°), 0.900 (20.1°), 0.982 (29.4°), 0.973 (40.1°) for water; 0.975 (10.4°), 0.780 (15.3°), 0.969 (29.4°), 0.874 (40.1°) for 10 mM KCl; 0.965 (10.4°), 0.986 (15.3°), 0.991 (20.1°), 0.965 (29.4°), 0.971 (40.1°) for 100 mM KCl.

has been experimentally observed and explained in a number of papers [57–61]. Systems which exhibit high interfacial tensions, like air–water, are especially affected by minute amounts of impurity. Intentional addition of surfactants to clean water has been demonstrated experimentally by various authors [12,17,56,62,63] to change the boundary condition at the air–liquid interface from mobile to partially or fully immobile thereby lowering the speed of a rising bubble.

3.3. Effect of salt concentration on the terminal velocity of the bubble

The most significant feature, observed for the first time to our knowledge, is that U_T is influenced by salt concentration of the medium. This behavior is particularly obvious at the angles of inclination between 1.6° and 4.2° as shown in Fig. 2 which reveals that U_T decreases with increase in the salt concentration. The trend becomes more pronounced in larger bubbles. Since salt at these concentrations has negligible effects on solution density or on the bubble's surface tension, these observations imply that the disjoining pressure due to double-layer interaction between the bubble and glass surface has an influence on U_T. This is consistent with the theoretical development of White and Carnie, which finds that a bubble's velocity is a function of its radius, the angle of inclination and the film thickness, h_o. As the salt concentration is increased, the range of electric double-layer repulsion decreases due to screening. This results in a decrease in h_o and an increase in viscous drag due to the thinner film between the bubble and glass surface.

The data for higher angles between 10.4° and 40.1°, shown in Fig. 3, on the other hand, does not show a clear dependence of speed with salt concentration. Note that correlation coefficients (R^2) of the trend lines at higher angles are smaller than those at lower angles. This could be due to two factors: First, the range of errors in speed and inclination at these angles is greater than that in the lower angles because the bubble images in this speed range are less clear. Second, the effect of hydrodynamic forces could become more dominant than the effect of disjoining pressure in higher speed ranges. In the next section, we discuss the influences of hydrodynamic and disjoining pressures on U_T by comparing the experimental results with two theories.

3.4. Comparison between experimental results and two theories

Two dimensionless numbers, the Bond number, B, and the capillary number, Ca, are used for convenience to compare experimental results with theories. For small bubbles, where surface tension dominates gravity (small B), the dependence of bubble velocity on bubble radius can be re-cast using dimensional analysis into a relationship between the Ca (a scaled velocity) and $B^{1/2}$. The Bond number is given by:

$$B = \frac{\Delta\rho g A^2}{\gamma} \tag{1}$$

in which γ is the surface tension. The Bond number represents the ratio of buoyancy forces to surface tension forces. Because the buoyancy force is proportional to the bubble area (which is a function of square radius, A^2), $B^{1/2}$ is proportional to bubble radius, A. Therefore $B^{1/2}$ can be considered as a dimensionless (scaled) radius.

The scaled velocity can be expressed in terms of the capillary number,

$$Ca = \frac{\eta U}{\gamma} \tag{2}$$

where η is the dynamic viscosity. The capillary number represents the ratio of viscous drag forces to surface tension forces. There are some reports in the literature that η may be different from the bulk viscosity at film thicknesses less than 2 nm [64,65], while other reports state that η remains the same as the bulk [66–69]. In this study, we employed the value of bulk viscosity for η since even if the claims of increased viscosity in thin films are correct, we are dealing with capillary numbers estimated for film thicknesses well above the thickness where the increase of viscosity has been claimed [64–69].

The relation between bubble radius and terminal velocity expressed in these dimensionless terms also allows us to compare our results with those of other systems, including experiments using different bubble sizes in various media such as viscous silicone oil [37], as will be shown later in Fig. 5a.

The theory of Hodges et al. [1] considers the steady state sedimentation under gravity of a viscous drop suspended in another liquid with a different viscosity along a gently inclined plane. It predicts a terminal velocity of bubbles/drops from the viscosity ratio λ of drops and media (for air bubbles, $\lambda \ll 1$). The theory

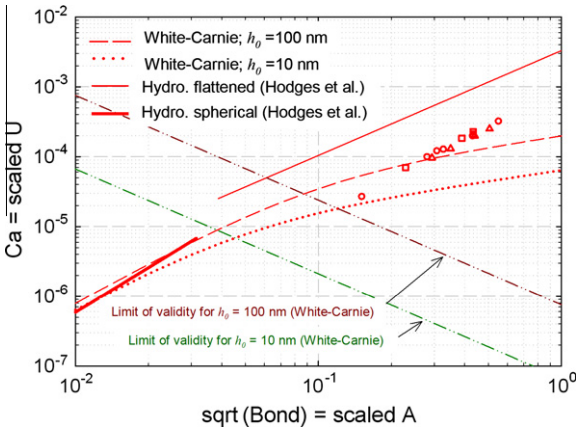

Fig. 4. Experimental and theoretical relationships between terminal velocity and bubble radius in dimensionless forms (capillary number, Ca, and square root of Bond number, $B^{1/2}$) for different salt concentrations (water [squares], 10 mM KCl [circles], and 100 mM KCl [triangles]) at an inclination angle of 2.1°. The thin and thick solid lines are predictions according to Hodges et al. [1] for spherical and flattened bubbles, respectively. The dashed and dotted lines are White and Carnie's theoretical predictions [2] for h_o = 100 and 10 nm. The limits of validity for each h_o are shown with dash-dotted lines.

determines the film thickness between a bubble and a solid plane from a normal force balance of buoyancy against hydrodynamic forces. Therefore, the predictions of Hodges et al. are of the form $Ca = f(B, \phi, \lambda)$ having different ranges of Bond number and viscosity ratio. They have shown that a three-dimensional drop, with low capillary number motion, may exhibit eleven asymptotically distinct types of motion, with the corresponding predicted shapes.

Of these, only two cases are relevant to our experiments: (Case 1) a slipping spherical bubble (denoted as the case SI_3 in their paper [1]) which occurs for $B < \phi^2$; and (Case 2) a slipping flattened bubble (their case $FIII_2$) for $\phi^2 < B < 1$.

The sliding velocity in dimensionless terms is given by:

$$Ca = \frac{10}{9} B\phi / \log\left(B^{-1}\phi^{-2}\right) \tag{3}$$

for very small bubbles, $B < \phi^2$; and

$$Ca = 0.474(B\phi^2)^{3/4} \tag{4}$$

for larger bubbles, $\phi^2 < B \leqslant 1$.

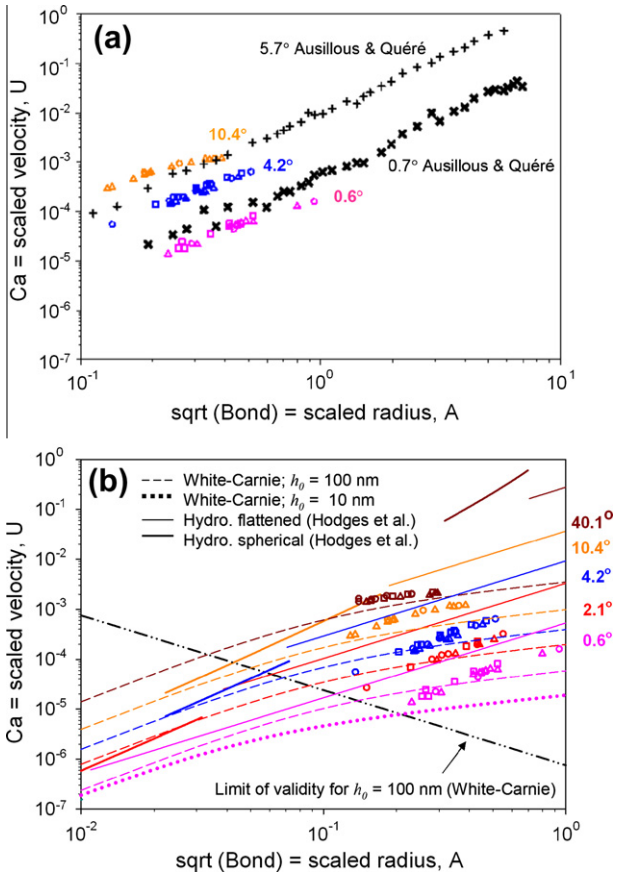

Fig. 5. Experimental and theoretical relationship between terminal velocity and bubble radius in dimensionless forms (capillary number, *Ca*, and square root of Bond number, $B^{1/2}$) for different angles of inclination in water (squares), 10 mM KCl (circles); and 100 mM KCl (triangles). (a) Experimental data for $\phi = 0.6°$ (pink), 4.2° (blue), and 10.4° (orange) and data reproduced from Aussillous and Quéré [31] for the corresponding angle as labelled are included (exes for $\phi = 0.7°$; crosses for $\phi = 5.7°$). (b) Experimental results for angles between 0.6° to 4.2°. Hodges's theoretical predictions are shown with solid lines (thick lines for hydrodynamic, spherical; thin lines for hydrodynamic, flattened shape). White and Carnie's theoretical predictions for $h_o = 100$ nm are shown with dashed lines, and for $h_o = 10$ nm with $\phi = 0.6°$ is shown with a dotted line. To make the plot less busy, we omitted the White–Carnie predictions for $h_o = 10$ nm at other angles. (For interpretation of the references to color in this figure legend, the reader is referred to the web version of this article.)

An alternative theory has been developed by White and Carnie [2]. In this theory it is assumed that an air bubble in liquid medium sliding along the underside of an inclined surface, has a flattened region separated from the wall by a uniform film thickness, h_o, which is not affected by hydrodynamic forces but is determined by a balance between buoyancy, surface tension and disjoining pressure, $\Pi(h_o)$. The functional form of the theory gives the predicted U_T in terms of A, h_o and ϕ: $U_T = f(A, \phi; h_o)$. The film thickness h_o can be expressed as a ratio to the radius

$$\varepsilon = \frac{h_o}{A}. \tag{5}$$

In terms of these dimensionless numbers, the theory can then be presented as $Ca = f(B, \phi, \varepsilon)$. Here we only show the resultant equations; the detailed derivation will be reported separately by White and Carnie [2]. For given values of h_o, the theory predicts a sliding velocity given in dimensionless terms by

$$Ca = (2/3)\frac{B\sin\phi}{\frac{1}{10}\log\left(\frac{3}{B}\right) + 1.708 + \frac{9\pi}{16\sqrt{2}}\left(\frac{B}{3}\right)^{1/2}\frac{1}{\varepsilon^{1/2}} - \frac{1}{2}\log(\varepsilon)} \tag{6}$$

The theory is only valid for velocities in the range given by:

$$Ca < \frac{32}{3\pi}\varepsilon^{3/2} \approx 3\varepsilon^{3/2}. \tag{7}$$

This domain of validity is derived as follows: assuming the bubble has the shape of a truncated sphere, the theory determines the hydrodynamic pressure distribution in the film between bubble and wall. Because the drop shape is assumed constant, the theory is only valid if the hydrodynamic pressure is much less than the disjoining pressure, which at equilibrium is just the Laplace pressure ($P_L = 2\gamma/A$). In the simplest case, the pressure is largest at the front entrance to the film, i.e. where the film just starts to deviate from the equilibrium thickness. The requirement that the maximum hydrodynamic pressure is less than the Laplace pressure becomes the restriction on *Ca* given by Eq. (7).

Fig. 4 shows a comparison between one set of experimental data at a fixed inclination angle ($\phi = 2.1°$) and the predictions of the two theories. We have employed 10 nm and 100 nm for the representative values of h_o for the White–Carnie theory as it is reasonable equilibrium separation determined by balancing the Laplace pressure of the bubble with the disjoining pressure. For example, using a standard approximation for double layer disjoining pressure gives $h_o = 125$ nm for a 1 mm bubble with estimated surface potentials of glass = −100 mV and bubble = −50 mV at 10^{-3} M, and $h_o = 30$ nm assuming surface potentials of glass = −50 mV and bubble = −5 mV at 10^{-5} M.

Strictly speaking, h_o should not be constant but increase slightly as bubble radius increases because the value of h_o comes from a balance between a repulsive disjoining pressure and the Laplace pressure. However, the effect is very weak as it is logarithmic in bubble radius (for example, as the radius increases from 0.1 to 1 mm, h_o increases by 23 nm). Hence we have shown White–Carnie theoretical curves with constant h_o (10, 100 nm) for simplicity. The limits of validity (which are below the dashed–dotted lines) of the White–Carnie theory at $h_o = 10$ and 100 nm are also shown in the figure. It can be seen that our experimental data are out of the regime of validity of this theory, that is, the sizes of the bubbles used are larger and/or the sliding velocities are faster than the regime of validity, hence we are not able to make a conclusive statement on whether hydrodynamic or electrostatic forces are dominant in influencing the motion of the bubble sliding parallel to the glass in liquid. Nevertheless, it is interesting to find that our experimental data fall in between the predictions of the hydrodynamic-dominant and the disjoining pressure-dominant theories. Following the White–Carnie theory for $h_o = 100$ nm (which is a reasonable

approximation for water since it is close to equilibrium separation at 10^{-5} M as described above) up to experimental values of B, it appears that the White–Carnie theoretical line will be closer to experimental data than the case of the flattened bubbles of Hodges et al.'s theory, which predicts much faster bubbles for the same bubble size. On the other hand, extrapolating an empirical power law fit to the experimental data for water at $\phi = 2.1°$ to where the theory is valid, a terminal velocity of ~0.9 mm/s can be estimated for a bubble radius of 0.23 mm, compared to a theoretical prediction of 2.2 mm/s, a discrepancy of around 2. Unfortunately, neither extrapolation is strictly valid.

The slope of the data in Fig. 4 is close to that of the hydrodynamic model, but the magnitudes differ by at least a factor of 5. Clearly, neither theory is capturing every feature of the data in the region of bubble radii investigated here. At very small radii, the theories are so close that it would be difficult to distinguish between them with any data.

Fig. 5a shows our experimental data for three different inclination angles together with experimental results reported by Aussillous and Quéré [31]. As Aussillous and Quéré examined bubbles in silicone oil sliding along an inclined surface in a gravity-driven system, it is interesting to compare their experimental data with ours at a similar range of inclination angles ($\phi < 10°$). It is observed that dimensionless terminal velocities in aqueous solutions are similar to those in silicone oil at similar inclination angles. The dimensionless terminal velocities at inclination angle of 0.6° in aqueous solutions are in the same order of magnitude as the results at 0.7° in silicone oil. The results at 5.7° in silicone oil fall between the air bubble data sets at 4.2° and 10.4° in aqueous solutions. Note however that the data of Aussillous and Quéré was obtained in region with $B > 1$ in which drops are expected to adopt a pancake shape, whereas our data corresponds to $B < 1$.

The present results at inclination angles from 0.6° to 10.4° (Fig. 5b) show the same tendency described for an inclination angle at 2.1° in Fig. 4. i.e., measured terminal velocities are closer to the predictions of the White and Carnie theory at smaller B (although the data are beyond the limit of validity) while closer to the theory of Hodges et al. for flattened bubbles at greater B.

It was seen in Fig. 2 that the measured velocities are reduced by the addition of electrolyte, which is qualitatively consistent with the White–Carnie model. Added electrolyte would decrease the range of electrical double-layer forces acting between the wall and the bubble surface, thereby reducing h_o and increasing viscous drag in the thin film. Hence this experimental observation gives some support to the White–Carnie conjecture that disjoining pressure should be included when modelling sliding velocity, especially at small inclination angles, although quantitatively White and Carnie predict a stronger influence of disjoining pressure than indicated by the present results.

The experimental results fall between the theories that consider only effects of hydrodynamics (Hodges et al.) or consider that contributions from disjoining pressure play a significant role in determining sliding velocity (White–Carnie); neither can accurately predict the behavior of a bubble sliding under gently inclined surfaces in aqueous solutions. In the light of our data we can now discuss the main effects that are missing from the two models.

The Hodges et al. model neglects disjoining pressure, which, as our data show, can have a noticeable effect at low B, where the Hodges theory is further away from the data that it is at large B. We note that White's theory assumes a constant bubble shape and a constant film thickness. The assumption of a constant bubble shape requires that the hydrodynamic pressure is much less than the disjoining pressure. This limits the theory to small velocities (Ca in dimensionless terms) with either very small bubbles or very small angles of inclination. White and Carnie assume that the film thickness h_o is determined only by disjoining pressure, ignoring hydrodynamic lift that would increase h_o, hence reduce drag and increase U_T. Including the lift effect would close the gap toward the experimental data. Furthermore, it may be that a change in the film profile due to the distribution of hydrodynamic pressure in the film should be accounted for. This type of film with non-uniform thickness has been observed and described in studies of lubrication by liquids [70,71]. Denkov et al. [72] have demonstrated the undulation of the film experimentally and theoretically for a surfactant-laden system of a bubble in a glass capillary tube whose inner diameter is 10% larger than the bubble diameter. Griggs et al. [38] have theoretically examined a deformable drop or bubble sliding near an inclined plane at low Reynolds number and reported non-uniform film thickness at medium (15°) to higher (75°) inclination angles. Denkov et al. [72] reported that the h_o becomes constant at very low velocities of Ca less than 10^{-6}, while another theoretical model by Saugey et al. [73] reported the onset of irregularity in the h_o at $Ca \sim 6.72 \times 10^{-4}$. As the White–Carnie theory assumes a constant bubble shape and a constant film thickness, the theory cannot apply for estimating the speed of a bubble in the region where the sliding bubble may bounce off the wall or when the film thickness is non-uniform. A model considering the region where bubbles slide and bounce has been reported by Podvin et al. [74].

The White–Carnie theory also assumes that the total drag is insensitive to the details of the shape at the rim where the flattened area joins the spherical surface of the remainder of the bubble. In the region just outside the rim, the disjoining pressure decays from its uniform value $\Pi(h_o)$ to zero, and the local curvature would not be constant (as for a spherical surface). Both the hydrodynamic and disjoining pressures are affected by the altered bubble shape in this region. Hence for better modelling, it might be necessary to go beyond the truncated sphere approximation and consider this region in more detail.

Finally, it is worth noting that both theories assume mobile interfaces: air–liquid for White–Carnie and liquid–liquid for Hodges et al. Any modification of this boundary condition would result in increased hydrodynamic drag and a reduced sliding velocity at all values of B. This would bring the Hodges model closer to the data. As discussed above, the speeds predicted from White–Carnie theory were higher than the experimental speeds extrapolated into the domain of validity of the theory, and so a partially or fully immobile interface may improve the fit in this region, but it would not bring the extrapolated theoretical curves closer to the data in the experimental region. The presence of surface contaminants, for example surfactants at low concentration, would render the fluid–fluid interface partially or fully immobile, and it may be that the higher interfacial energy of air–water compared to silicone oil–water makes the bubbles more susceptible to contamination than the oil drops. An alternative mechanism that attributes surface immobilisation to electrokinetic effects that couple ion distribution to the flow field has been proposed by Yaminsky et al. [59,60]. A consequence of this coupling is that interfacial tension would be spatially inhomogeneous, with surface tension gradients influencing the flow field (a form of Marangoni effect). This would add considerable complexity to the modelling.

4. Conclusions

Terminal velocities of single bubbles sliding along the underside of an inclined surface have been measured in water and aqueous KCl solutions. The bubble size, angle of inclination, and salt concentration were all varied and their effects on the bubble terminal velocity were determined. We observed, particularly at the angle range of ~1–5°, that bubble terminal velocity is not only influenced by the bubble size and angle of inclination, but also by the salt

concentration of the media. This shows that the terminal velocity is influenced by disjoining pressure, which in this case is dominated by electrostatic double-layer forces. The data were compared with two theories: predictions from a hydrodynamic model by Hodges et al., and predictions from a model that includes disjoining pressure effects (considering electrostatic double-layer forces) by White and Carnie. Although our experimental results are beyond the regime where the White–Carnie theory is valid, the experimental results are closer to this theory with smaller bubbles, but vary with bubble size in a way that it more consistent with Hodges et al.'s theory. The overall conclusion is that neither theory contains all of mechanisms that are acting to determine the terminal velocity of bubbles sliding past a solid wall.

Acknowledgments

The authors wish to thank Darren Faulkner and Phil Souter for their technical assistance in the fabrication of the sliding bubble apparatus; and Stan Miklavcic for helpful discussions. This work was supported by the Australian Research Council (ARC) Special Research Centre for Particle and Material Interfaces, and Discovery Project DP0986371.

References

[1] S.R. Hodges, O.E. Jensen, J.M. Rallison, J. Fluid Mech. 512 (2004) 95.
[2] L.R. White, S.L. Carnie, J. Fluid Mech., MS ID JFM-11-S-0604, submitted for publication.
[3] P.G. Saffman, J. Fluid Mech. 1 (1967) 27.
[4] T. Maxworthy, C. Gnann, M. Kurten, F. Durst, J. Fluid Mech. 321 (1996) 421.
[5] A. Sam, C.O. Gomez, J.A. Finch, Int. J. Miner. Process. 47 (1996) 177.
[6] D. Rodrigue, D.D. Kee, C.F.C.M. Fong, J. Non-Newtonian Fluid Mech. 66 (1996) 213.
[7] A. Tomiyama, I. Kataoka, I. Zun, T. Sakaguchi, JSME Int. J. Ser. B 41 (1998) 472.
[8] R. Krishna, M.I. Urseanu, J.M.V. Baten, J. Ellenberger, Int. Commun. Heat Mass Transfer 26 (1999) 781.
[9] A. Margaritis, D.W.T. Bokkel, D.G. Karamanev, Biotechnol. Bioeng. 64 (1999) 257.
[10] I. Leifer, R.K. Patro, P. Bowyer, J. Atmos. Oceanic Technol. 17 (2000) 1392.
[11] J. Ortiz-Villafuerte, Y.A. Hassan, W.D. Schmidl, Exp. Therm. Fluid Sci. 25 (2001) 43.
[12] A. Tomiyama, G.P. Celata, S. Hosokawa, S. Yoshida, Int. J. Multiphase Flow 28 (2002) 1497.
[13] M. Krzan, K. Malysa, Colloids Surf., A: Physicochem. Eng. Aspects 207 (2002) 279.
[14] A.W.G.d. Vries, A. Biesheuvel, L.v. Wijngaarden, Int. J. Multiphase Flow 28 (2002) 1823.
[15] P.D. Marco, W. Grassi, G. Memoli, Int. J. Therm. Sci. 42 (2003) 435.
[16] G.P. Celata, M. Cumo, F.D. Annibale, A. Tomiyama, Int. J. Multiphase Flow 30 (2004) 939.
[17] S.S. Alves, S.P. Orvalho, J.M.T. Vasconcelos, Chem. Eng. Sci. 60 (2005) 1.
[18] K. Malysa, M. Krasowska, M. Krzan, Adv. Colloid Interface Sci. 114–115 (2005) 205.
[19] A. Zaruba, D. Lucas, H.-M. Prasser, T. Hohne, Chem. Eng. Sci. 62 (2007) 1591.
[20] G.P. Celata, F. D'Annibale, p.D. Marco, G. Memoli, A. Tomiyama, Exp. Therm. Fluid Sci. 31 (2007) 609.
[21] L. Parkinson, R. Sedev, D. Fornasiero, J. Ralston, J. Colloid Interface Sci. 322 (2008) 168.
[22] J. Li, V. Bulusu, N.R. Gupta, Chem. Eng. Sci. 63 (2008) 3766.
[23] E.E. Zukoski, J. Fluid Mech. 25 (1966) 821.
[24] Y. Taitel, A.E. Dukler, AlChE J. 22 (1976) 47.
[25] P.L. Spedding, V.T. Nguyen, Chem. Eng. Sci. 33 (1978) 987.
[26] M.E. Weber, A. Alarie, Chem. Eng. Sci. 41 (1986) 2235.
[27] T. Maxworthy, J. Fluid Mech. 229 (1991) 659.
[28] J. Masliyah, R. Jauhari, M. Gray, Chem. Eng. Sci. 49 (1994) 1905.
[29] M. Cook, M. Behnia, Int. J. Heat Fluid Flow 22 (2001) 543.
[30] C.E. Shosho, M.E. Ryan, Chem. Eng. Sci. 56 (2001) 2191.
[31] P. Aussillous, D. Quéré, Europhys. Lett. 59 (2002) 370.
[32] A.J. Addlesee, P.A. Kew, Trans. IChemE Part A 80 (2002) 272.
[33] K.M. DeBisschop, M.J. Miksis, D.M. Eckmann, Phys. Fluids 14 (2002) 93.
[34] D.M. Eckmann, D.P. Cavanagh, Colloids Surf., A: Physicochem. Eng. Aspects 227 (2003) 21.
[35] N.A. Inogamov, A.M. Oparin, J. Exp. Theor. Phys. 97 (2003) 1168.
[36] C.E. Norman, M.J. Miksis, Physica D 209 (2005) 191.
[37] A. Perron, L.I. Kiss, S. Poncsak, Int. J. Multiphase Flow 32 (2006) 606.
[38] A.J. Griggs, A.Z. Zinchenko, R.H. Davis, Int. J. Multiphase Flow 34 (2008) 408.
[39] B. Podvin, S. Khoja, F. Moraga, A. Attinger, Chem. Eng. Sci. 63 (2008) 1914.
[40] A.S. Najafi, Z. Xu, J. Masliyah, Can. J. Chem. Eng. 86 (2008) 1001.
[41] A.J. Griggs, A.Z. Zinchenko, R.H. Davis, Phys. Fluids 21 (2009) 093303:1.
[42] C.G. Pantano, Rev. Solid State Sci. 3 (1989) 379.
[43] M. Kosmulski, Chemical Properties of Material Surfaces, Surfactant Science Series, vol. 102, Marcel Dekker, New York, Marcel Dekker, New York, 2001.
[44] H.A. McTaggart, Philos. Mag. 27 (1914) 297.
[45] T. Alty, Proc. R. Soc. London, A 106 (1924) 315.
[46] S. Usui, H. Sasaki, H. Matsukawa, J. Colloid Interface Sci. 81 (1981) 80.
[47] K. Okada, Y. Akagi, M. Kogure, N. Yoshioka, Can. J. Chem. Eng. 68 (1990) 393.
[48] A. Graciaa, G. Morel, P. Saulner, J. Lachaise, R.S. Schechter, J. Colloid Interface Sci. 172 (1995) 131.
[49] G.H. Kelsall, S. Tang, S. Yurdakul, A.L. Smith, J. Chem. Soc., Faraday Trans. 92 (1996) 3887.
[50] K.A. Karraker, C.J. Radke, Adv. Colloid Interface Sci. 96 (2002) 34.
[51] P. Creux, J. Lachaise, A. Graciaa, J.K. Beattie, J. Phys. Chem. C 111 (2007) 3753.
[52] A.L. Perron, L.I. Kiss, S. Poncsak, Int. J. Multiphase Flow 32 (2006) 1311.
[53] L.A. Del Castillo, S. Ohnishi, R.G. Horn, J. Colloid Interface Sci. 356 (2011) 316.
[54] C.C. Maneri, N. Zuber, Int. J. Multiphase Flow 1 (1974) 623.
[55] J.J.J. Chen, Z. Jianchao, Q. Kangxing, B.J. Welsh, M.P. Taylor, Rise velocity of air bubbles under a slightly inclinded plane submerged in water, Presented at 5th Asian Congress of Fluid Mechanics, Korea, 1992.
[56] R. Clift, J.R. Grace, M.E. Weber, Bubbles, Drops, and Particles, Academic Press, London, 1978.
[57] G. Marrucci, Chem. Eng. Sci. 24 (1969) 975.
[58] G.H. Kelsall, S. Tang, A.L. Smith, S. Yurdakul, J. Chem. Soc., Faraday Trans. 92 (1996) 3879.
[59] V.V. Yaminsky, S. Ohnishi, E.A. Vogler, R.G. Horn, Langmuir 26 (2010) 8061.
[60] V.V. Yaminsky, S. Ohnishi, E.A. Vogler, R.G. Horn, Langmuir 26 (2010) 8075.
[61] R.G. Horn, L.A. Del Castillo, S. Ohnishi, Adv. Colloid Interface Sci. (2011), doi:10.1016/j.cis.2011.05.006.
[62] A. Frumkin, V.G. Levich, Zh. Fiz. Khim. 21 (1974) 1183.
[63] R.B. Fdhila, P.C. Duineveld, Phys. Fluids 8 (1996) 310.
[64] Y. Zhu, S. Granick, Phys. Rev. Lett. 87 (2001) 096104.
[65] H. Sakuma, K. Otuki, K. Kurihara, Phys. Rev. Lett. 96 (2006) 046104.
[66] J.N. Israelachvili, J. Colloid Interface Sci. 110 (1986) 263.
[67] R.G. Horn, D.T. Smith, W. Haller, Chem. Phys. Lett. 162 (1989) 404.
[68] U. Raviv, S. Giasson, J. Frey, J. Klein, J. Phys.: Condens. Matter 14 (2002) 9275.
[69] U. Raviv, J. Klein, Science 297 (2002) 1540.
[70] D. Dowson, G.R. Higginson, Elasto-hydrodynamic lubrication, in: The Fundamentals of Roller and Gear Lubrication, Pergamon Press, Oxford, 1966.
[71] A.D. Roberts, D. Tabor, Proc. R. Soc. London, A 325 (1971) 323.
[72] N.D. Denkov, S. Tcholakova, K. Golemanov, Colloids Surf., A: Physicochem. Eng. Aspects 282–283 (2006) 329.
[73] A. Saugey, W. Drenckhan, D. Weaire, Phys. Fluids 18 (2006) 053101.
[74] B. Podvin, S. Khoja, F. Moraga, D. Attinger, Chem. Eng. Sci. 63 (2008) 1914.